Comput Geosci
DOI 10.1007/s10596-016-9578-z

ORIGINAL PAPER

Oxidation wave structure and oxygen breakthrough for air injection into light oil reservoirs

F. P. Santos[1] · **A. A. Mailybaev**[2] · **D. Marchesin**[2]

Received: 20 November 2015 / Accepted: 16 May 2016

Abstract This paper combines analytical and numerical studies of light oil recovery by air injection. We investigate in detail the internal structure of oxidation fronts in two-phase flow in a porous medium, taking into account reaction, vaporization, and condensation of liquid fuel, with longitudinal heat conduction. Our solution shows that between regimes of total and partial oxygen consumption there is a change in the oxidation wave, which may have negative implications for oxygen breakthrough in light oil recovery process. In spite of the simplifications used to derive the analytical solution, the latter agrees with direct numerical simulations. Finally, based on our analytical solution, we provide a phase diagram to predict conditions for total or partial oxygen consumption in light oil recovery process.

Keywords Porous medium · Travelling wave · Oxygen breakthrough · Oxidation wave struture · Light oil recovery

1 Introduction

Air injection leading to in situ combustion is generally considered applicable to recovery of heavy oils because, e.g., it causes a significant reduction in oil viscosity, which improves the oil extraction of the reservoirs. Notwithstanding, it can be also used to recover light oils by mechanisms such as combustion gas drive, distillation, and thermal expansion. Several combustion models were proposed for describing in situ combustion theoretically and experimentally, e.g., [1, 5–9, 12, 24, 27, 28, 36]. Most of them assume coke to be the source of energy to sustain in situ combustion through high temperature oxidation, although heat can also be produced through oxidation of a liquid phase at medium temperature. There are also papers that focus on numerical simulation of the combustion process [2–4, 11, 15, 21, 23, 28, 37].

The mechanisms actually responsible for oil displacement in the combustion process vary with the type of oil and temperature. There is high temperature oxidation (HTO) [30, 31], in which cracking occurs forming coke, which is subsequently oxidized at high temperatures, and low temperature oxidation (LTO), in which the oxygen is absorbed or incorporated by the hydrocarbon molecules to form alcohols, aldehydes, acids, or other oxygenated hydrocarbons [16, 17, 19]. The LTO may be followed by complete scission of molecules into small reaction products such as water, CO, or CO_2 [14, 17, 18, 22].

There has been recent progress in the development of the mathematical theory for the recovery mechanism of light oil by air injection at medium pressures [32, 33], which was confirmed by numerical simulations [20] and by laboratory experiments [22]. Note that air injection can be very effective even in heterogeneous light oil reservoirs, as the oil evaporates away from low permeability parts to be collected at higher mobility streaks. The oxidation process is characterized by a medium temperature oxidation (MTO) wave [32]. In this wave, various physical processes, i.e., reaction, vaporization, condensation, and filtration take place. The name of the wave originates from the fact

✉ F. P. Santos
fsantos@eq.ufrj.br
✉ A. A. Mailybaev
alexei@impa.br
✉ D. Marchesin
marchesi@impa.br

[1] Escola de Química, Universidade Federal do Rio de Janeiro, Rio de Janeiro, RJ 21941-909, Brazil

[2] Instituto Nacional de Matemática Pura e Aplicada – IMPA, Rio de Janeiro, RJ, Brazil

Published online: 01 June 2016

that the maximum temperature cannot exceed the boiling temperature of the liquid oil at elevated pressure. Thus, temperatures required for the cracking process are not reached preventing the transition to HTO.

In our work, we consider the model proposed in [32] focusing on the longitudinal thermal conduction effects, in order to identify their influence in the internal structure of the medium temperature oxidation wave. We emphasize that there are no transversal heat losses in this model. Previous numerical studies in [20, 23] considered rather low injection rates and obtained a solution with three nonlinear waves: the thermal, oxidation, and saturation waves. Our purpose is to perform analytical and numerical studies of light oil recovery by air injection and investigate the effects of injection rates varying from low to high. For the first time, the effect of oxygen breakthrough in light oil recovery is described analytically, which is a relevant contribution for the petroleum engineering discipline. We show that when diffusive and capillary effects are neglected, low injection rates lead to complete oxygen consumption in a small region of highest temperatures. On the other hand, when the injection rate increases, incomplete oxygen consumption in the reaction can occur due to decrease in oxygen residence time. The main conclusion is that increasing air injection rate changes significantly the internal oxidation wave structure, possibly causing oxygen breakthrough, which has negative implications for the light oil recovery process. Thus, it is crucial to prevent oxygen breakthrough as it increases the explosion risk in the production well.

Section 2 describes the physical model, first in dimensional way and then dimensionless variable are used in the rest of the work. In the Section 3 analytical approximations for the oxidation wave profile are obtained. These are ordinary differential equations solved analytically in Section 4 under some simplifications. Section 5 presents an example for heptane modeling light oil. Section 6 shows comparison of theoretical results with numerical simulations. Finally, we end with some conclusions and remarks.

2 Model formulation

We investigate the oxidation front in two-phase flow originating from the injection of a gaseous oxidizer (air) is into porous rock initially filled with liquid fuel (light oil). As our main application, we consider light oil recovery by air injection (as opposed to in-situ combustion for heavy oil recovery), but other applications, e.g., cleaning up soils, can be considered. In this case, the temperature is bounded by the boiling point of the liquid and, thus, remains relatively low.

In our model, we disregard gaseous phase chemical reactions [25]. When oxygen reacts with liquid hydrocarbons at low temperatures, a series of reactions may occur that convert hydrocarbons into oxygenated hydrocarbons (ketone, alcohols, and aldehyde) [13]. Further oxidation leads to complete scission of the hydrocarbons. In this paper, the combination of reaction to oxygenated hydrocarbons with the subsequent reaction to gaseous products is simplified in the form of a single reaction modeled as

$$\nu_l(\text{hydrocarbons}) + O_2 \rightarrow \nu_g\,(\text{gaseous products}), \tag{1}$$

i.e., one mole of oxygen reacts with ν_l moles of initially present (liquid) hydrocarbons, generating ν_g moles of gaseous products (H_2O, CO_2, etc.), which are taken as inert. In this model, all hydrocarbons are grouped into a single pseudo-component and air is totally immiscible in the liquid phase. Thus, the differences in physical properties of the liquid due to changes of its composition can be disregarded (density, viscosity, boiling temperature, etc.). We neglect water that may be present initially or that condenses from the reaction products, and typically favors the oil recovery [20].

We study one-dimensional flow in the positive spatial direction x of two phases, a liquid and a gas. The liquid has saturation s_l, describing the fraction of pore volume occupied by the liquid. The gas saturation is, therefore, $s_g = 1 - s_l$. In the gaseous phase, we distinguish the molar fraction of the hydrocarbon Y_h from the molar fraction of oxygen Y_o. The remaining components with fraction lumped into $Y_r = 1 - Y_h - Y_o$ consist of gaseous reaction products and inert components from the injected gas. The liquid and gas molar densities are indicated by ρ_l and ρ_g, respectively. The molar balance equations for the liquid and for the three gaseous pseudo-components are [32]:

$$\frac{\partial}{\partial t}\varphi\rho_l s_l + \frac{\partial}{\partial x}u_l\rho_l = -\nu_l W_r - W_v, \tag{2}$$

$$\frac{\partial}{\partial t}\varphi Y_h\rho_g s_g + \frac{\partial}{\partial x}u_{gh}\rho_g = W_v, \tag{3}$$

$$\frac{\partial}{\partial t}\varphi Y_o\rho_g s_g + \frac{\partial}{\partial x}u_{go}\rho_g = -W_r, \tag{4}$$

$$\frac{\partial}{\partial t}\varphi Y_r\rho_g s_g + \frac{\partial}{\partial x}u_{gr}\rho_g = \nu_g W_r. \tag{5}$$

The reaction and vaporization rates W_r and W_v are defined in Eqs. 17 and 18 below.

Neglecting capillary pressure effects, the liquid (u_l), gas (u_g), and total (u) Darcy velocities have the form

$$u_l = -k\frac{k_{rl}}{\mu_l}\frac{\partial P}{\partial x}, \quad u_g = -k\frac{k_{rg}}{\mu_g}\frac{\partial P}{\partial x}, \quad u = u_l + u_g \tag{6}$$

with the viscosities μ_l, μ_g, absolute permeability k and pressure P. The relative phase permeability functions are chosen as

$$k_{rl} = \left(\frac{s_l - s_l^r}{1 - s_l^r}\right)^2 \quad \text{for } s_l \geq s_l^r, \quad \text{and} \quad 0 \quad \text{otherwise;} \tag{7}$$

$$k_{rg} = (1 - s_l)^2, \tag{8}$$

where s_l^r is the residual liquid hydrocarbon saturation, while the residual gas saturation is assumed to be zero. The temperature dependence of the gas and liquid viscosities μ_g and μ_l in cP is chosen as in [34] (for T in Kelvin):

$$\mu_g = \frac{7.5}{T + 120}\left(\frac{T}{291}\right)^{3/2}, \quad \mu_l = 0.0132 \exp\left(\frac{1006}{T}\right) \tag{9}$$

which correspond to air and heptane.

It is convenient to express the Darcy velocities of liquid u_l and gas u_g in Eqs. 2–5 as

$$u_l = u f_l, \quad u_g = u f_g = u - u_l, \tag{10}$$

where the liquid and gas fractional flow functions are given in term of relative permeabilities and viscosities as

$$f_l = \frac{k_{rl}/\mu_l}{k_{rl}/\mu_l + k_{rg}/\mu_g}, \quad f_g = 1 - f_l. \tag{11}$$

Neglecting molecular diffusion, the Darcy velocities for the gas components in Eqs. 3–5 are

$$u_{gj} = u_g Y_j \qquad (j = h, o, r). \tag{12}$$

Taking the sum of Eqs. 3–5, using Eq. 12 and recalling the identity $Y_h + Y_o + Y_r = 1$, we obtain the equality $u_{gh} + u_{go} + u_{gr} = u_g$ as well as the balance law for the total gas as

$$\frac{\partial}{\partial t}\varphi \rho_g s_g + \frac{\partial}{\partial x} u_g \rho_g = (\nu_g - 1) W_r + W_v. \tag{13}$$

Assuming that the temperature of the solid rock, the liquid, and the gas are equal at each time and position (local thermodynamic equilibrium), we can write the energy balance equation as

$$\begin{aligned} &\frac{\partial}{\partial t}\left(C_m + \varphi c_l \rho_l s_l + \varphi c_g \rho_g s_g\right)\Delta T \\ &+ \frac{\partial}{\partial x}(c_l u_l \rho_l + c_g u_g \rho_g)\Delta T \\ &= \lambda \frac{\partial^2 T}{\partial x^2} + Q_r W_r - Q_v W_v, \end{aligned} \tag{14}$$

where Q_v is the latent heat of vaporization, Q_r is the heat of reaction and $\Delta T = T - T_{res}$, with initial reservoir temperature T_{res}. In Eq. 14, the heat capacities C_m, c_l, c_g are taken as constants, which is a good approximation and facilitates the analysis. We neglect heat losses, which are usually very small in field applications (however, taking into account heat losses becomes essential for interpreting laboratory experiments).

For the gas phase, we use the law of ideal gases to define

$$\rho_g = P/RT. \tag{15}$$

The partial pressure $Y_h^{eq} P$ of the gaseous hydrocarbon in liquid–gas equilibrium can be approximated by the Clausius-Clapeyron relation written as

$$Y_h^{eq} P = P_{atm} \exp\left(-\frac{Q_v}{R}\left(\frac{1}{T} - \frac{1}{T_{bn}}\right)\right), \tag{16}$$

where T_{bn} is the (normal) boiling point of the liquid hydrocarbon measured at atmospheric pressure P_{atm}. This relation determines the equilibrium fraction of gaseous hydrocarbon Y_h^{eq}. Taking $Y_h^{eq} = 1$ in Eq. 16, one recovers the actual boiling temperature $T = T_b$ at pressure P of the hydrocarbon considered.

The vaporization/condensation rate in the two-phase region is approximated by

$$W_v = k_v \varphi (Y_h^{eq} - Y_h) \rho_g s_l, \tag{17}$$

where k_v is the vaporization/condensation rate constant and Y_h^{eq} is given in Eq. 16. Note that Eq. 17 represents both physical phenomena, either vaporization ($Y_h < Y_h^{eq}$) or condensation ($Y_h > Y_h^{eq}$). This formulation can be considered as a consequence of non-equilibrium thermodynamics, see for instance [25, 35]. We assume that k_v is very large, describing the situation close to local thermodynamic equilibrium for the gaseous hydrocarbon mole fraction Y_h, i.e., assuming that vaporization and condensation are instantaneous.

For the reaction, one usually employs a rate equation of the form

$$W_r = A_r \varphi \rho_l s_l \left(\frac{P Y_o}{P_{atm}}\right) \exp\left(-\frac{T_{ac}}{T}\right), \tag{18}$$

with pre-exponential factor A_r and activation temperature $T_{ac} = E_{ac}/R$. The reaction rate becomes large at elevated temperatures. However, the reaction is assumed to be much slower than the vaporization and condensation.

A similar model was studied in [33], where the heat conduction term $\lambda \partial^2 T/\partial x^2$ in Eq. 14 was neglected. However, we will see that this term is important for determining the oxidation wave profile.

2.1 Dimensionless equations

In order to give us insight into what might be small parameters that could be neglected in our analytical solution,

we reformulate our system of equations in terms of the dimensionless quantities below.

$$\tilde{t}=\frac{t}{t^*},\quad \tilde{x}=\frac{x}{x^*},\quad \theta=\frac{T-T_{res}}{\Delta T^*},\quad \tilde{u}=\frac{u}{\varphi v^*},\quad \tilde{p}=\frac{P}{P^*},\quad \tilde{\rho_g}=\frac{\rho_g}{\rho_g^*}, \tag{19}$$

where the reference variables, which are denoted by an asterisk, are:

$$t^*=\frac{x^*}{v^*},\quad x^*=\frac{\lambda}{C_m v^*},\quad v^*=\frac{Q_r\left(\rho_g u\right)_{inj} Y_o^{inj}}{C_m \Delta T^*}, \tag{20}$$

$$\rho_g^*=\frac{P^*}{RT_{res}},\quad \Delta T^*=T_b^*-T_{res},\quad \mu^*=\mu_g(T_{res}). \tag{21}$$

The dimensionless variable θ describes the temperature distribution; the reservoir initial condition is $\theta=0$. We define the boiling temperature T_b^* at pressure P^*, where the reference pressure P^* is chosen to be convenient in each case. Hence, the value $\theta=1$ corresponds the boiling temperature at $\tilde{p}=1$. The air injection rate $\left(\rho_g u\right)_{inj}$ is considered to be constant and the reference quantities t^* , x^*, and v^* are obtained by considering a wave whose reaction heat raises the rock temperature to T_b^*. We will use the following dimensionless parameters:

$$\alpha_l=\frac{\varphi c_l \rho_l}{C_m},\quad \alpha_g=\frac{\varphi c_g \rho_g^*}{C_m},\quad \gamma=\frac{Q_v}{Q_r},\quad \beta=\frac{\rho_g^*}{\rho_l}, \tag{22}$$

$$a_r=\frac{t^* A_r \rho_l P^*}{\rho_g^* P_{atm}},\quad \sigma=\frac{\rho_g^* v^* \varphi}{\left(\rho_g u\right)_{inj}},\quad \kappa_v=k_v t^*,$$
$$\Omega=\frac{kP^*}{x^*\mu^*\varphi v^*}, \tag{23}$$

$$\theta_0=\frac{T_{res}}{\Delta T^*},\quad \theta_{ac}=\frac{T_{ac}}{\Delta T^*},\quad \theta_h=\frac{Q_v}{R\Delta T^*}. \tag{24}$$

The governing system of equations for our model is transformed using the dimensionless variables described above (omitting tildes) to

$$\frac{\partial}{\partial t}s_l+\frac{\partial}{\partial x}u f_l=-\beta(\nu_l w_r+w_v), \tag{25}$$

$$\frac{\partial}{\partial t}Y_h S_g+\frac{\partial}{\partial x}uY_h F_g=w_v, \tag{26}$$

$$\frac{\partial}{\partial t}Y_o S_g+\frac{\partial}{\partial x}uY_o F_g=-w_r, \tag{27}$$

$$\frac{\partial}{\partial t}S_g+\frac{\partial}{\partial x}u F_g=(\nu_g-1)w_r+w_v, \tag{28}$$

$$\frac{\partial}{\partial t}(1+\alpha_l s_l+\alpha_g S_g)\theta$$
$$+\frac{\partial}{\partial x}u(\alpha_l f_l+\alpha_g F_g)\theta=\frac{\partial^2\theta}{\partial x^2}+\frac{\sigma(w_r-\gamma w_v)}{Y_o^{inj}}, \tag{29}$$

where

$$\rho_g=\frac{p}{1+\theta/\theta_0},\quad S_g=(1-s_l)\rho_g,\quad F_g=(1-f_l)\rho_g. \tag{30}$$

The five balance laws (25)–(29) describe the flow in terms of the dependent variables θ, s_l, Y_o, Y_h, and u. The dimensionless forms of vaporization and reaction rates are given by

$$w_v=\kappa_v(Y_h^{eq}-Y_h)\rho_g s_l, \tag{31}$$

$$w_r=a_r p s_l Y_o \exp\left(-\frac{\theta_{ac}}{\theta+\theta_0}\right), \tag{32}$$

with the equilibrium fraction

$$Y_h^{eq}=\frac{\mathcal{Y}(\theta)}{p},\quad \mathcal{Y}(\theta)=\exp\left(\frac{\theta_h}{\theta_0+1}-\frac{\theta_h}{\theta_0+\theta}\right). \tag{33}$$

The dimensionless pressure can be found by integrating

$$\frac{\partial p}{\partial x}=-\frac{u}{\Upsilon},\quad \Upsilon(\theta,s_l)=\left(\frac{k_{rl}}{\mu_l/\mu^*}+\frac{k_{rg}}{\mu_g/\mu^*}\right)\Omega, \tag{34}$$

which is derived from Eq. 6, with boundary condition defined at the recovery side.

Note that according to Eq. 11, the fractional flow function $f_l(s_l,\theta)$ has an S-shaped form in the variable s_l with a single inflection point and the limiting values $f_l(0,\theta)=0$, $f_l(1,\theta)=1$ for purely gaseous and purely oleic flow. Typical liquid and gas viscosities satisfy $d\mu_l/d\theta<0$ and $d\mu_g/d\theta>0$, see Eq. 10. These inequalities together with Eq. 11 yield

$$\frac{\partial f_l(s_l,\theta)}{\partial\theta}\geq 0. \tag{35}$$

In order to facilitate the analysis and shorten the formula of the final analytical solution, we introduce the following simplifications in the model. We assume that there exists no net gas production in the reaction. We also consider the vaporization and condensation as the dominant source term in the liquid phase balance compared to the oxidation. We neglect the vaporization heat compared to the energy released by the reaction. These simplifications lead the following parameter values:

$$\nu_g=1,\quad \nu_l=0,\quad \gamma=0. \tag{36}$$

Due to the small oxidation wave speed compared to the gas velocity, to the small ratio between the gas and the liquid density, see Eqs. 22 and 23, and low initial reservoir temperature, we will assume that

$$\sigma\ll 1,\quad \beta\ll 1,\quad \mathcal{Y}(0)\ll 1, \tag{37}$$

where the last inequality implies that initially there is a very small fraction of gaseous hydrocarbon at the initial temperature in the reservoir.

3 Oxidation wave

In the oxidation wave, pressure variations are assumed to be small compared to the prevailing pressure. Under this condition, the pressure P is approximately constant along the wave with a value denoted by P_w. Although this pressure changes in time, this change is slow compared to the oxidation processes within the wave and a quasi-stationary approach can be used to analyze this wave. Therefore, we are allowed to choose a constant pressure $P = P_w$ to be the reference quantity P^*, leading to the non-dimensional value $p = 1$. We also assume that the oxidation wave has a stationary profile moving with constant speed v. Then the profile for the oxidation wave can be written in terms of a single independent traveling coordinate, $\xi = x - vt$.

We can distinguish the vaporization from the condensation region in the oxidation wave, Fig. 1. The vaporization region is located on the upstream part, where the hot injected gas meets the liquid and the vapor hydrocarbon fraction increases from $Y_h = 0$ to the equilibrium value Y_h^{eq}. The vaporization region is very thin (compared to the reaction and thermal conduction zones in the condensation region) under the assumption of fast vaporization. In particular, it represents a jump in Y_h if the vaporization is assumed to be instantaneous. We can neglect the change of temperature in this very thin region, so that $\theta \approx \theta^u$. Recall that the vaporization heat was neglected in Eq. 36; otherwise, a small increase of temperature occurs [32].

The dimensionless balance laws, (25)–(29), for the travelling wave profile in the frame of reference, $\xi = x - vt$, become

$$\frac{d}{d\xi}\psi_l = -\beta w_v, \tag{38}$$

$$\frac{d}{d\xi}\psi_g Y_h = w_v, \tag{39}$$

$$\frac{d}{d\xi}\psi_g Y_o = -w_r, \tag{40}$$

$$\frac{d}{d\xi}\psi_g = w_v, \tag{41}$$

$$\frac{d}{d\xi}(-v\theta + \alpha_l\theta\psi_l + \alpha_g\theta\psi_g) = \frac{d^2\theta}{d\xi^2} + \frac{\sigma w_r}{Y_o^{inj}}, \tag{42}$$

where we used conditions (36) and introduced the liquid and gas fluxes in the moving reference frame as

$$\psi_l = uf_l - vs_l, \quad \psi_g = uF_g - vS_g. \tag{43}$$

Using Eqs. 43 and 30 with $p = 1$, one can check that the following equality relating the fluxes in the moving reference frame, ψ_l and ψ_g, is satisfied:

$$\psi_g(1 + \theta/\theta_0) = u - v - \psi_l. \tag{44}$$

The upstream condition for the oxidation wave corresponds to air injection in the reservoir with no oil, Fig. 1. Here, the temperature θ^u is elevated due to the heat released by oxidation. The condition for the gas flux, uF_g, is obtained by approximating its value by a constant in the region between the injection point and the oxidation wave, as it follows from Eq. 28 with vanishing source terms and negligible time derivative, see e.g. [32]. At the injection region, the oil flux vanishes, $f_l = 0$, and Eqs. 30, 19, and 23

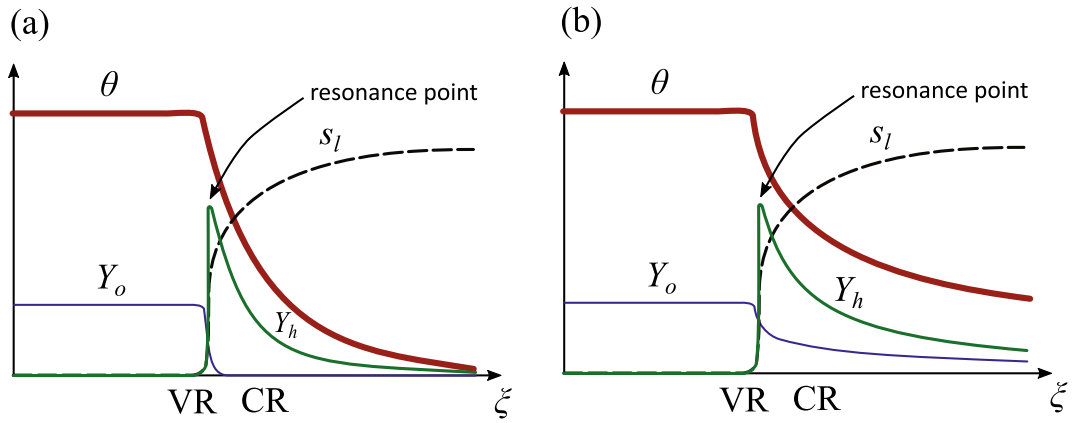

Fig. 1 Schematic structure of the wave profile with the vaporization region (VR) and condensation region (CR) showing the temperature θ, oil saturation s_l, the oxygen fraction Y_o and the hydrocarbon fraction Y_h in the gas phase: **a** complete oxygen consumption at highest temperatures followed by an exponential decrease of temperature downstream, **b** oxygen breakthrough leading to a long logarithmic tail downstream. The flow direction is from the left to the right

yield the dimensionless value $uF_g = 1/\sigma$. We summarize this boundary condition as

$$\xi \to -\infty: \quad \theta = \theta^u, \quad s_l = Y_h = 0, \quad Y_o = Y_o^{inj}, \\ uF_g = \frac{1}{\sigma}. \tag{45}$$

The downstream condition describes the reservoir with oil in equilibrium with its vapor at the initial reservoir temperature:

$$\xi \to +\infty: \quad \theta = 0, \quad s_l = s_l^d > 0, \quad Y_h = \mathcal{Y}(0), \\ Y_o = 0, \quad u = u^d. \tag{46}$$

The conditions (45) and (46) contain the unknown temperature θ^u on the upstream side and the unknown oil saturation s_l^d and the gas speed u^d on the downstream side. The wave speed v also has to be found.

3.1 Limiting states of oxidation wave

In order to find the limiting states in Eqs. 45 and 46, we substitute w_v and w_r from Eqs. 39 and 40 into Eqs. 42, 38 and 41, yielding

$$\frac{d}{d\xi}\left(-v\theta + \alpha_l\theta\psi_l + \alpha_g\theta\psi_g - \frac{d\theta}{d\xi} + \frac{\sigma\psi_g Y_o}{Y_o^{inj}}\right) = 0, \tag{47}$$

$$\frac{d}{d\xi}\left(\psi_l + \beta\psi_g Y_h\right) = 0, \tag{48}$$

$$\frac{d}{d\xi}\left(\psi_g(1 - Y_h)\right) = 0. \tag{49}$$

These equations above still represent the balance laws for our system of equations. However, as we are first interested in the limiting states of the oxidation wave, this new system of equations can be used directly for obtaining the upstream and downstream conditions in the oxidation wave. Integrating the equations above with respect to ξ from $-\infty$ to ∞ with boundary conditions (45) and (46) yields

$$-v\theta^u + \alpha_l\theta^u\psi_l^u \\ +\alpha_g\theta^u\psi_g^u + \sigma\psi_g^u = 0, \tag{50}$$

$$\psi_l^u = \psi_l^d + \beta\psi_g^d\mathcal{Y}(0), \tag{51}$$

$$\psi_g^u = \psi_g^d(1 - \mathcal{Y}(0)). \tag{52}$$

As outcome, we have three algebraic equations for the limiting states, where $\psi_{l,g}^u$ and $\psi_{l,g}^d$ denote the fluxes (43) at the upstream and downstream sides.

Using the upstream boundary condition (45), where $s_l = 0$ and $f_l = 0$ due to lack of oil, from Eq. 43, we find

$$\psi_l^u = 0, \quad \psi_g^u = \frac{1}{\sigma} - \frac{v}{1 + \theta^u/\theta_0} \approx \frac{1}{\sigma}, \tag{53}$$

where the last relation follows from condition (37) because $v \sim 1$ by the chosen of the reference quantities. The downstream fluxes are found by solving Eqs. 51 and 52 in terms of ψ_l^d and ψ_g^d, and using Eqs. 53 and 37 as

$$\psi_l^d = -\frac{\beta\mathcal{Y}(0)}{\sigma(1 - \mathcal{Y}(0))} \approx -\frac{\beta\mathcal{Y}(0)}{\sigma}, \\ \psi_g^d = \frac{1}{\sigma(1 - \mathcal{Y}(0))} \approx \frac{1}{\sigma}. \tag{54}$$

Finally, by substituting Eq. 53 into Eq. 50, we obtain the expression for upstream temperature,

$$\theta^u = \left(v - \frac{\alpha_g}{\sigma}\right)^{-1}. \tag{55}$$

Substituting Eq. 54 into Eq. 44 computed on the downstream side (46) with the simplifications (37), we derive an equation for downstream Darcy velocity,

$$u^d = \psi_l^d + \psi_g^d + v = \frac{1 - \beta\mathcal{Y}(0)}{\sigma} + v \approx \frac{1}{\sigma}. \tag{56}$$

The first expression in Eq. 43 computed on the downstream side (46) with Eqs. 54 and 56 yields the nonlinear equation for the saturation s_l^d as

$$\frac{f_l(s_l^d, 0)}{\sigma} - vs_l^d = -\frac{\beta\mathcal{Y}(0)}{\sigma}. \tag{57}$$

We obtained the three Eqs. 55, 56, and 57, which determine the oxidation temperature θ^u and the downstream state s_l^d and u^d, provided that the wave speed v is known. It will be obtained in the following section.

3.2 Wave speed

The set of balance laws are not enough to determine the limiting states at upstream and downstream states, since in the moving reference frame the wave speed is an extra variable. To determine the oxidation wave speed, integration of Eqs. 47–49 is performed in the semi-infinite interval from $-\infty$ to ξ, which leads to

$$\left(-v + \alpha_l\psi_l + \alpha_g\psi_g\right)\theta - \frac{d\theta}{d\xi} + \frac{\sigma\psi_g Y_o}{Y_o^{inj}} = 0, \tag{58}$$

$$\psi_l + \beta\psi_g Y_h = 0, \tag{59}$$

$$\psi_g(1 - Y_h) = \tfrac{1}{\sigma}, \tag{60}$$

where the constants on the right-hand side correspond to the left-hand side expressions evaluated at $\xi \to -\infty$ using condition (45) and Eqs. 53 and 55. From Eqs. 59 and 60, we obtain the gas and liquid flux in the moving reference frame.

$$\psi_g = \frac{1}{\sigma(1 - Y_h)}, \quad \psi_l = -\frac{\beta Y_h}{\sigma(1 - Y_h)}. \tag{61}$$

Substituting Eq. 61 into Eq. 44, we derive an expression for

$$u = \frac{1 + \theta/\theta_0 - \beta Y_h}{\sigma(1 - Y_h)} + v \approx \frac{1 + \theta/\theta_0}{\sigma(1 - Y_h)}, \tag{62}$$

where we used conditions (37).

Using Eq. 61 in the definition of ψ_l in Eq. 43, we obtain

$$u f_l(\theta, s_l) - v s_l = -\frac{\beta Y_h}{\sigma(1 - Y_h)}. \tag{63}$$

It was shown in [32] that Eq. 63 allows a continuous wave profile if the following condition

$$v = \left(u \frac{\partial f_l}{\partial s_l}\right)_r \tag{64}$$

is satisfied at the point "r", separating the vaporization and condensation regions, Fig. 1. This equation represents the resonance condition, i.e., the coincidence of the oxidation wave speed v with the characteristic speed, $u\,(\partial f_l/\partial s_l)$, of the saturation (Buckley–Leverett) wave.

At the resonance point, we have $\theta \approx \theta^u$ and $Y_h = \mathcal{Y}(\theta^u)$, which follow from the small size of vaporization region and the equilibrium condition, as we wrote above in this section. Then the gas speed is given by Eq. 62. Hence, the system of two Eqs. 63 and 64 can be solved with respect to the two unknown, v and s_l, providing the wave speed v and the oil saturation s_l at the resonance point.

4 Wave profile

Detailed structure of the wave profile, including localization of the oxidation reaction with possible oxygen breakthrough, is the main result of our paper and it will be derived in this section. For this purpose, we rewrite Eq. 58. First, we isolate the temperature derivative in Eq. 58, next we replace the terms ψ_g and ψ_l from Eq. 61, and finally, we express v from Eq. 55 in terms of θ^u. This procedure yields an expression for dimensionless temperature in the moving reference frame,

$$\frac{d\theta}{d\xi} = -\frac{\theta}{\theta^u} - \frac{(\alpha_l\beta - \alpha_g)\, Y_h}{\sigma\,(1 - Y_h)}\theta + \frac{Y_o}{Y_o^{inj}\,(1 - Y_h)}. \tag{65}$$

Similarly, Eq. 40 with ψ_g from Eq. 61 and w_r from Eq. 32 with $p = 1$ is written as

$$\frac{d}{d\xi}\left(\frac{Y_o}{1 - Y_h}\right) = -\sigma a_r s_l Y_o \exp\left(-\frac{\theta_{ac}}{\theta + \theta_0}\right). \tag{66}$$

Although the expressions above represent the whole recovery domain, we are actually interested in the condensation region, where most of the reaction occurs. Here, the equilibrium condition yields $Y_h = \mathcal{Y}(\theta)$ and the saturation s_l is given by Eq. 63. The latter equation possesses two roots and the large one must be chosen [33].

We split our analysis into two parts. First, let us consider the oxygen consumption mechanism in the region of highest temperatures $\theta \approx \theta^u$. In this region, we can write Eqs. 65 and 66 approximately as

$$\frac{d\theta}{d\xi} = -K_1 + \eta, \tag{67}$$

$$\frac{d\eta}{d\xi} = -K_2 s_l \eta \exp\left(-\frac{\theta_{ac}}{\theta + \theta_0}\right), \tag{68}$$

where the new variable η, which essentially represents the fraction of the oxygen that is consumed in the reaction, is defined as

$$\eta = \frac{Y_o}{Y_o^{inj}(1 - \mathcal{Y}(\theta^u))}, \tag{69}$$

and the constants K_1 and K_2 below are only defined to compact Eqs. 66 and 65,

$$K_1 = 1 + \frac{(\alpha_l\beta - \alpha_g)\,\mathcal{Y}(\theta^u)}{\sigma\,(1 - \mathcal{Y}(\theta^u))}\theta^u, \tag{70}$$

$$K_2 = \sigma a_r \left(1 - \mathcal{Y}(\theta^u)\right). \tag{71}$$

In the derivation of Eqs. 67 and 68, we kept the temperature dependence of the Arrhenius term due to large θ_{ac}, which leads to strong temperature dependence, while $\theta = \theta^u$ and $Y_h = \mathcal{Y}(\theta^u)$ is assumed in the other terms.

As we already mentioned, the reaction can be neglected in the vaporization region, where the oxygen flux in Eq. 40 is approximated as $\psi_g Y_o \approx Y_o^{inj}/\sigma$ according to the upstream conditions (45). With ψ_g from Eq. 61, this procedure yields $\eta = 1$ at the resonance point according to Eq. 69.

In order to find a solution, we divide Eq. 68 by Eq. 67, and as consequence, we have a relation between the oxygen consumption and temperature below,

$$\frac{d\eta}{d\theta} = \frac{K_2 s_l \eta}{K_1 - \eta} \exp\left(-\frac{\theta_{ac}}{\theta + \theta_0}\right). \tag{72}$$

Linearizing the exponential expression in Eq. 72 near the maximum temperature θ^u yields

$$-\frac{\theta_{ac}}{\theta + \theta_0} \approx -\frac{\theta_{ac}}{\theta^u + \theta_0} + Z_l(\theta - \theta^u), \tag{73}$$

where the Zeldovich number

$$Z_l = \frac{\theta_{ac}}{(\theta^u + \theta_0)^2} \gg 1 \tag{74}$$

is large due to the high activation energy. Thus, a small temperature decrease

$$\delta\theta \sim 1/Z_l \ll 1 \tag{75}$$

leads to a considerable decrease of the Arrhenius exponential term. According to Eq. 67, this temperature change occurs in a small space interval,

$$\delta\xi \sim \frac{\delta\theta}{|K_1|} \sim \frac{1}{Z_l\,|K_1|}. \tag{76}$$

As the behavior of the right-hand side of Eq. 72 is dominated by the strong exponential dependence on θ, the change of the oil saturation has minor importance, and we can take it constant $s_l = s_l^r$ with the value at the resonance point. Hence, Eq. 72 with the above simplifications reads

$$\frac{d\eta}{d\theta} \approx \frac{C Z_l \eta}{K_1 - \eta} e^{Z_l(\theta - \theta^u)}, \tag{77}$$

where

$$C = \frac{K_2 s_l^r}{Z_l} \exp\left(-\frac{\theta_{ac}}{\theta^u + \theta_0}\right). \tag{78}$$

Writing Eq. 77 as

$$\left(\frac{K_1}{\eta} - 1\right) d\eta = C Z_l e^{Z_l(\theta - \theta^u)} d\theta \tag{79}$$

and integrating in the region of highest temperatures $\theta_1 \le \theta \le \theta^u$ with the corresponding interval $\eta_1 \le \eta \le 1$ yields

$$-K_1 \log \eta_1 - 1 + \eta_1 = C - C e^{Z_l(\theta_1 - \theta^u)} \approx C, \tag{80}$$

where the term with $e^{Z_l(\theta_1 - \theta^u)} \ll 1$ can be neglected due to the large value of Z_l. Equation 80 determines the value of η_1, which can be used in Eq. 69 to find the oxygen fraction that passes unburned through the highest temperature region as

$$Y_o^{unb} = Y_o^{inj} \left(1 - \mathcal{Y}(\theta^u)\right) \eta_1. \tag{81}$$

When $Y_o^{unb} \ll Y_o^{inj}$, most of oxygen is consumed in a thin region of high temperatures. In this case, we can take $Y_o = 0$ and assume the equilibrium condition, $Y_h = \mathcal{Y}(\theta)$, downstream in the condensation region. Then, Eq. 65 can be integrated as

$$\xi = \xi_0 + \int_\theta^{\theta^u} \left(\frac{1}{\theta^u} + \frac{\left(\alpha_l \beta - \alpha_g\right) \mathcal{Y}(\vartheta)}{\sigma \left(1 - \mathcal{Y}(\vartheta)\right)}\right)^{-1} \frac{d\vartheta}{\vartheta}, \tag{82}$$

where the constant ξ_0 denotes the location of the high-temperature reaction region in a chosen reference frame. Equation 82 determines implicitly the temperature profile $\theta(\xi)$. Since the integral is dominated by the factor $d\vartheta/\vartheta$, we have a fast nearly exponential decay of the temperature in the condensation region, Fig. 1a.

Otherwise, if Y_o^{unb} is significant, the oxygen propagates to the region of lower temperatures. When the low-temperature reaction is not negligible, a long reaction tail may appear [10]. This is typically the case in our study, due to relatively low activation energy of the light oil oxidation combined with elevated reservoir temperatures [13]. In this case, we can determine the shape of the reaction tail approximately by neglecting the derivative $d\theta/d\xi$ (a long tail implies small spatial derivatives) in Eq. 65 and assume equilibrium condition $Y_h = \mathcal{Y}(\theta)$. This yields

$$Y_o = Y_o^{inj} \left(1 - \mathcal{Y}(\theta)\right) \left(\frac{1}{\theta^u} + \frac{\left(\alpha_l \beta - \alpha_g\right) \mathcal{Y}(\theta)}{\sigma \left(1 - \mathcal{Y}(\theta)\right)}\right) \theta. \tag{83}$$

At low temperatures, $\mathcal{Y}(\theta) \ll 1$, and we can simplify Eq. 83 as

$$Y_o \approx \frac{Y_o^{inj} \theta}{\theta^u}. \tag{84}$$

Therefore, the equation for the temperature profile can be determined from Eqs. 66 and 84 as

$$\frac{Y_o^{inj}}{\theta^u} \frac{d\theta}{d\xi} = -\sigma a_r s_l^d \left(\frac{Y_o^{inj} \theta}{\theta^u}\right) \exp\left(-\frac{\theta_{ac}}{\theta + \theta_0}\right), \tag{85}$$

where we again used $Y_h \approx \mathcal{Y}(\theta) \ll 1$ and took into account the downstream value $s_l = s_l^d$ of the oil saturation. By integrating Eq. 85, we obtain the following implicit expression for the temperature profile

$$\xi = \xi_0 + \frac{1}{a_r \sigma s_l^d} \int_\theta^{\theta^u} \exp\left(\frac{\theta_{ac}}{\vartheta + \theta_0}\right) \frac{d\vartheta}{\vartheta}. \tag{86}$$

Due to large value of θ_{ac}, the integral on the right-hand side of Eq. 86 is dominated by the large exponential term (until θ becomes very small). This domination causes the exponential decrease of ξ with increasing θ, or equivalently, slow logarithmic decay of $\theta(\xi)$. The oxygen fraction profile follows the same scenario due to Eq. 84. Therefore, a long logarithmic tail is formed, which is associated with oxygen breakthrough into the region of low temperatures, Fig. 1b.

5 Example: oxygen consumption for in situ oxidation of heptane

To demonstrate the theory developed so far on a specific example, we use the reservoir data given in Table 1, which corresponds to air injection at various pressures and rates

Table 1 Values of dimensional reservoir parameters for heptane as a liquid fuel [32]

Q_r	=	400 kJ/mol	T_{ini}	=	300 K	λ	=	3 W/m K
Q_v	=	31.8 kJ/mol	T_{bn}	=	371 K	k_v	=	1.0 1/s
$(\rho_g u)_{inj}$	=	0.01 − 1000.0 kmol/m^2/day	T_b	=	$T_b(P_{res})$	s_l^r	=	0.25
C_m	=	2 MJ/m^{3}K	T_{ac}	=	7066 K	A_r	=	4060 1/s
c_g	=	29 J/mol K	P_{res}	=	10 − 100 bar	ν_l	=	0.090 [mol/mol]
c_l	=	224 J/mol K	φ	=	0.3	ν_g	=	1.36 [mol/mol]
ρ_l	=	6826 mol/m^3	Y_o^{inj}	=	0.21	k	=	10^{-9} m^2

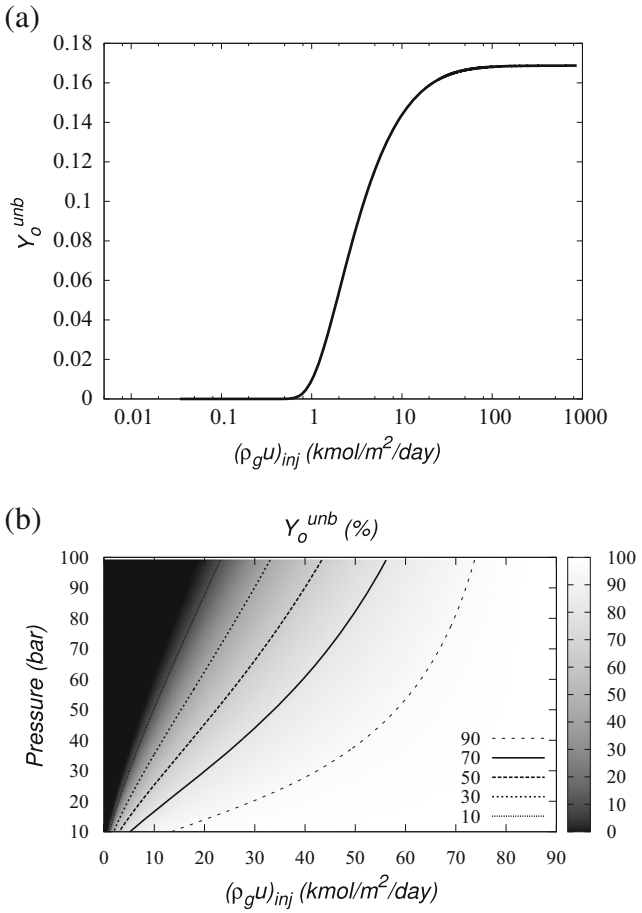

Fig. 2 **a** Unburned oxygen fraction Y_o^{unb} in the high-temperature region as function of air injection rate for reservoir pressure $P_{res} = 10$ bar. **b** Unburned oxygen fraction in % of total oxygen at different injection rates and pressures

into porous rock containing heptane modeling a single pseudo-component light oil. As experimental data on oxidation rates at low temperatures in porous media is very limited, parameter values for the reaction kinetics are chosen to be compatible with experimental results obtained in [13].

Figure 2a shows the fraction of oxygen Y_o^{unb} passing unburned through the high-temperature region, which was computed at pressure 10 bar using Eq. 81 as described in Section 4. One can see that as air injection rate increases from low to high values, the oxidation mechanism in the high-temperature region undergoes a continuous change from total oxygen consumption for $(\rho_g u)_{inj} \lesssim 1$ kmol/m^2/day to partial oxygen consumption and then to complete oxygen breakthrough for $(\rho_g u)_{inj} \gtrsim 20$ kmol/m^2/day. Note that the right limiting value of the curve in Fig. 2a corresponds to complete oxygen breakthrough (no oxygen consumption) in the high-temperature region. One should not be confused with the fact that this limiting value is different from the initial fraction $Y_o^{inj} = 0.21$ in the injected air, because the vaporization process contributes to the gas mixture altering the oxygen fraction from its initial value to a lower value.

Figure 2b shows the dependence of the unburned oxygen fraction Y_o^{unb} on both, air injection rate and pressure. One can see that the oxygen consumption increases for higher pressures, so that the oxygen breakthrough region is shifted to higher injection rates. This occurs due to increase of reaction rate with pressure, see Eq. 18, while larger injection rates reduce oxygen residence time.

Below we consider two specific cases corresponding to the air injection rates of 0.138 (case I) and 13.8 kmol/m^2/day (case II), both at pressure of 10 bar. The first case corresponds to total oxygen consumption, while the second case describes a oxidation regime with almost no oxygen burned at high temperatures, see Fig. 2. These two cases correspond, respectively, to the injection Darcy velocities of 0.07 and 34 m/day. In applications, where Darcy velocity decreases with distance from the injection well, these cases may correspond to the oxidation process far from or close to the injection well. We first present the theoretical results and then compare them with direct numerical simulations in the section that follows.

Theoretical predictions for the oxidation wave speed and upstream/downstream states are obtained by solving numerically Eqs. 63, 64 and 55, which determine the dimensionless values of θ^u, v and s_l^r. Next, the oil saturation s_l^d downstream of the wave is found from Eq. 57. The resulting dimensional values v (m/day), T^u (in Kelvin) and s_l^d are listed in the second column of Table 2, which will be compared with the values obtained from direct numerical simulations.

Table 2 Comparison of theoretical prediction for oxidation wave speed v and limiting states T^u, s_l^d with direct numerical simulations for the full model (FM) and the simplified model (SM) in the cases I and II

Variable	Analytical	FM simulation	SM simulation
Case I			
v (m/day)	0.0125	0.0116	0.0112
T^u (K)	397	385	395
s_l^d	0.52	0.51	0.52
Case II			
v (m/day)	6.21	5.9	6.07
T^u (K)	397	417	412
s_l^d	0.52	0.5	0.5

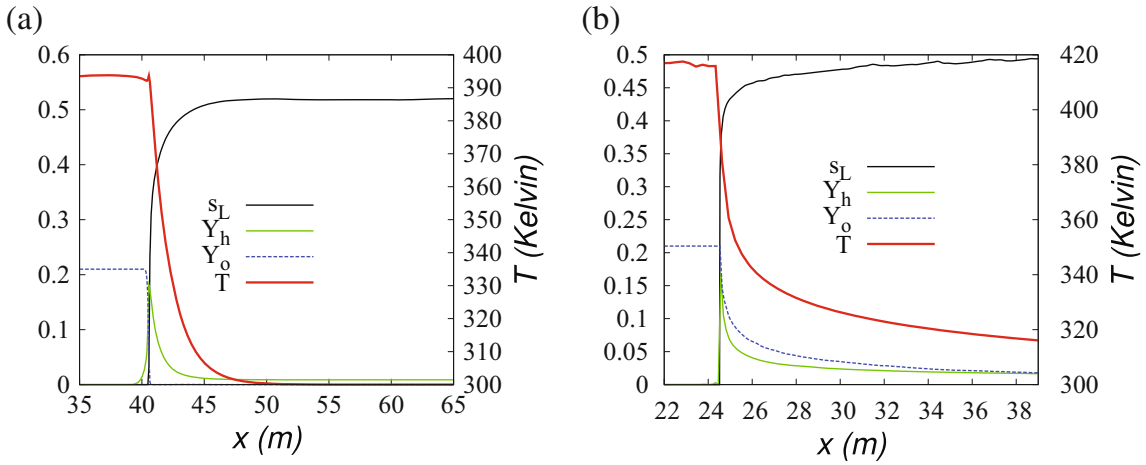

Fig. 3 Results of numerical simulations: **a** Case I with low air injection rate, when all oxygen is consumed at high temperatures. **b** Case II with high air injection rate leading to oxygen breakthrough and long low-temperature tail in the wave profile. Shown are the liquid saturation s_l, molar fractions Y_h and Y_o (hydrocarbon and oxygen) in gaseous phase and the temperature T at fixed times. The temperature is indicated at the right axis; other variables vary between 0 and 1 as indicated at the left axis

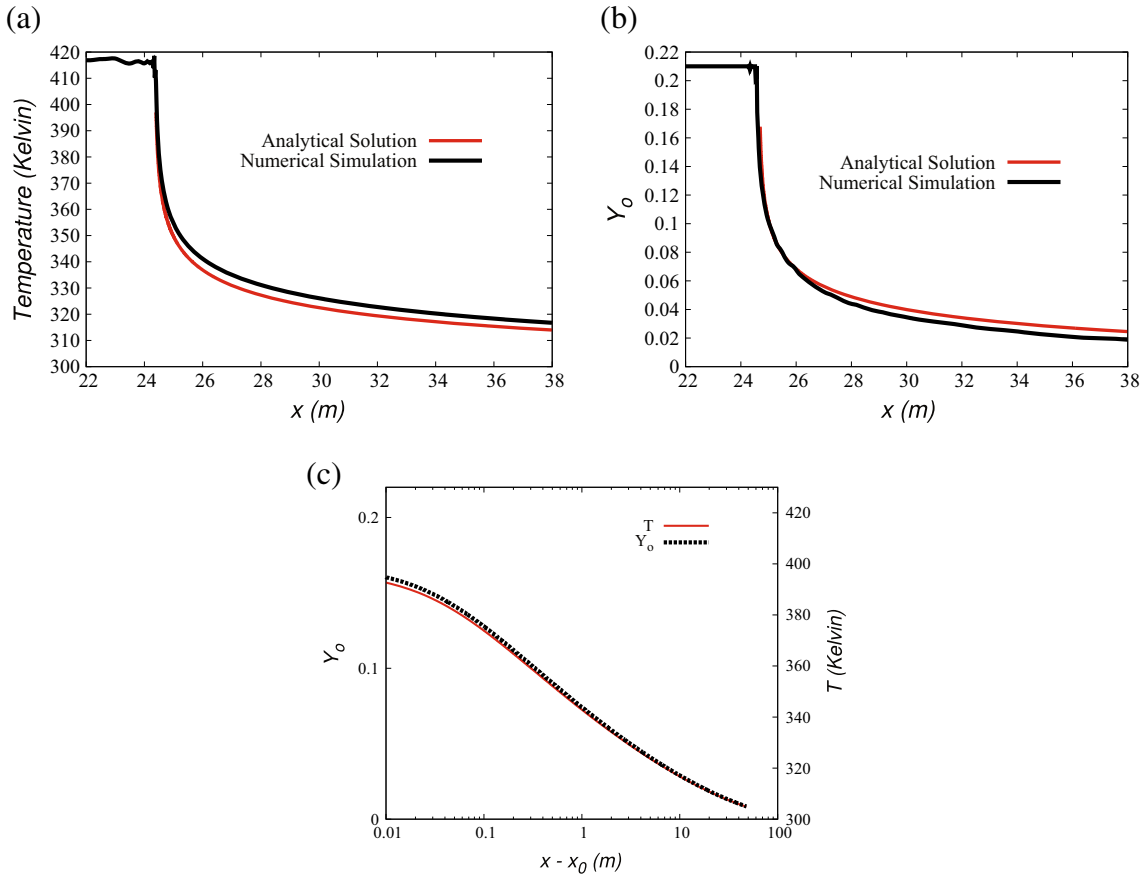

Fig. 4 Comparison of the wave profile obtained analytically (*red curves*) with direct numerical simulations (*black curves*) in the case II corresponding to a high air injection rate. **a** The temperature T and **b** the oxygen fraction Y_o in gaseous phase. **c** Graphs of analytical solutions with logarithmic horizontal scale, where $x_0 = 24.7$ m is the location of high-temperature region

6 Comparison with numerical simulations

We performed numerical simulations for the example of the previous section. For this purpose, we used a central finite difference scheme in space and the backward implicit method in time with an adaptive time step control [26] for all equations except for Eq. 6, which is calculated explicitly. This discretization yields a system of nonlinear equations at each time step, which is solved by the inexact Newton method [29]. In order to derive an equation for pressure, (87), we multiply Eq. 2 by ρ_g/ρ_l and combine it with Eq. 13. Equation 87 is treated separately from the rest of the system but also using backward implicit method and inexact Newton method.

Namely, at each time step, the system of Eqs. 2, 3, 4, and 14 is solved for a fixed Darcy velocity profile and pressure from a previous time step. Then, Eq. 87 is solved separately only for pressure p, as the gas density ρ_g is a function of p, see Eq. 30. As a splitting technique, Eq. 87 solution is carried out with all other variables fixed, except for pressure. Finally, the Darcy velocity is computed by means of Eq. 6.

$$\varphi\,(1-s_l)\,\frac{\partial \rho_g}{\partial t}+u(1-f_l)\frac{\partial \rho_g}{\partial x}\;=\;\left(\frac{\rho_g}{\rho_l}\nu_l+\nu_g-1\right)W_r \\ +\left(1-\frac{\rho_g}{\rho_l}\right)W_v \\ -\rho_g\frac{\partial u}{\partial x} \qquad (87)$$

For our simulations, we used a spatial grid step of 0.1 m, which is fine enough to capture the multi-scale processes.

We take the initial reservoir conditions in the form

$$t\;=\;0,\quad x\geq 0:\quad T=T^{ini},\quad s_l=s_l^{ini}R(x), \\ Y_h\;=\;Y_h^{eq},\quad Y_o=0, \qquad (88)$$

where $R(x)$ is a ramp function. These conditions correspond to a cold reservoir filled with oil at saturation s_l^{ini} and a gas phase, which is in equilibrium with the oleic phase and contains no oxygen. The boundary conditions at $x\;=\;0$ (injection side) are

$$s_l=Y_l=0,\quad T=T^{ini},\quad \rho u=(\rho u)_{inj},\quad Y_o=Y_o^{inj}. \qquad (89)$$

The boundary conditions at $x=L$ are chosen as

$$\partial_x s_l W=\partial_x Y_o=\partial_x Y_h=\partial_x T=0,\quad P=P_{res}, \qquad (90)$$

featuring the fixed pressure P_{res} at the recovery side.

Numerical simulations were carried out for two values of injection rate corresponding to cases I and II. A steady oxidation wave was produced after a while in both cases. The wave profiles are shown in Fig. 3 for representative time values, when the oxidation process is stabilized. The pressure variations were small (not shown in the figures), with the prevailing pressure close to P_{res}. The temperature increases from the initial value of 300 K to the maximum value of 385 K in case I (420 K in case II) at the downstream side of the oxidation wave. One can distinguish a thin region at upstream side of the oxidation wave, where the oil is vaporized leading to a peak of the respective gaseous fraction Y_h. Further downstream, there is a wide region where the oil condenses while temperature decreases. The oil saturation s_l increase abruptly, as a result of oil vaporization and condensation processes along the wave, reaching the downstream value of $s_l^d=0.52$ in case I ($s_l^d=0.5$ in case II).

The oxidation wave speed and limiting states obtained in numerical simulations are presented in Table 2 ("FM simulation" column) and show good agreement with the theoretical predictions. A deviation can be partially attributed to the simplifications used in order to obtain the analytical solution. We confirm this fact with a different simulation ("SM simulation" column in Table 2), where the most significant simplifications given by Eq. 36 are included in the numerical model. The values obtained in such simulations are indeed closer to the theoretical ones.

Note that the oxidation wave speed, 0.0125 m/day in case I (6.21 m/day in case II), is only about six times smaller than the air injection Darcy speed, which equals 0.07 m/day (34 m/day in case II). Together with the jump in the oil saturation from zero to a relatively high value $s_l^d\;\approx\;0.5$ at the downstream side, these properties contribute to the efficiency of the oil recovery mechanism in the oxidation wave. The main difference between the cases I and II, predicted theoretically and observed numerically, is that all oxygen is consumed at high temperatures in case I, while the oxygen spreads over the wide condensation region, thus, penetrating deep into the cold zone in case II.

Finally, let us analyze the details of the oxygen and temperature profiles in the case II, demonstrating the slow logarithmic decay into the downstream cold zone, as it was concluded from the analysis in Section 4. The analytic solution for these profiles obtained from the integration of Eq. 86 is shown in Fig. 4a, b (red line). That solution is superimposed with the results of numerical simulations showing good agreement. Figure 4c presents the analytic solution with the logarithmic horizontal scale, demonstrating nearly linear decay in the central part. As we already mentioned, this implies slow logarithmic decay for both oxygen and temperature profiles.

7 Conclusion

In this work, we studied the oxidation process in a porous medium to assess the effect of the air injection rate in light oil recovery. The model used allows some essential insights

of how the injection rate can change the oxidation wave structure. Based on our results, we state that this change in the wave structure occurs due to the oxygen breakthrough and leads to a long logarithmic tail downstream of the wave. From the simulations, one can see that at low injection rates, the oxygen is consumed completely within a short distance. However, when the air injection rate is high, oxygen propagates a long distance inside the oil containing region. This is undesirable due to the danger of oxygen breakthrough at the production well.

With some extra simplifications in the model, we derived an analytical solution and obtained the condition for the oxygen is totally consumed in a region of highest temperatures. The analytical and numerical solutions agree with reasonable accuracy, as shown in Table 2 and Fig. 4. In addition, we show the phase diagram describing the oxidation regimes of total and partial oxygen consumption based on the two parameters: air injection rate and pressure. Thus, we can conclude that this analytical approach is suitable to predict and control the oxygen consumption in the light oil recovery process, and therefore, it is able to identify the explosion risk in the production well. Note that the main advantage of our approach over the numerical solution is that, while the numerical simulation can require a large computational resource, our solution is simple enough to be determined with a very low computational cost.

Acknowledgments The work was supported by the CNPq (302351/2015-9, 402299/2012-4 301564/2009-4 and 470635/2012-6), by the FAPERJ (E-26/210.738/2014, E-26/201.210/2014, E-26/110.658/2012, E-26/111.369/2012, E-26/110.114/2013, E-26/010.002762/2014, E-26/210.874/2014). F.P. Santos also acknowledges the support from IMPA/CAPES fellowship.

Nomenclature

A_r	Oxidation reaction pre-exponential factor, $1/s$
i	Liquid (l) and gas (g) phases
c_i	Heat capacity of phase i (l or g), $J/(molK)$
C_m	Heat capacity of porous matrix, $J/(m^3K)$
f_i	Fractional flow function of phase i
k	Rock permeability, m^2
k_{ri}	Relative permeability of phase i
P_{res}	Reservoir pressure, Pa
Q_r	Oxidation reaction enthalpy per mole of oxygen at reservoir temperature, $J/(mol)$
Q_v	Latent heat of vaporization at reservoir temperature, $J/(mol)$
R	Ideal gas constant, $J/(molK)$
s_i	Saturation of phase i
T	Temperature, K
T_{bn}	Normal boiling temperature of oil, K
T^{ini}	Initial reservoir temperature, K
T^{ac}	Oxidation activation temperature, K
u_i	Darcy velocity of phase i, m/s
u_{gj}	Darcy velocity of component of hydrocarbons (h), oxygen (o) and remaining components (r) in the gas phase, m/s
u_{inj}	Darcy velocity of injected gas, m/s
W_r	Oxidation reaction rate, $mol/(m^3s)$
W_v	Vaporization/condensation rate, $mol/(m^3s)$
x, t	Spatial coordinate, m, and time, s
Y_o, Y_h, Y_r	Molar fractions: hydrocarbons (h), oxygen (o) and remaining components (r), mol/mol
Y_o^{inj}	Oxygen fraction in injected gas
φ	Porosity
λ	Thermal conductivity of porous medium, $W/(mK)$
μ_i	Viscosity of phase i, Pas
ν_l, ν_g	stoichiometric coefficients in the oxidation reaction
ρ_i	Molar density of phase i, mol/m^3

References

1. Abou-Kassem, J.H., Farouq Ali, S.M., Ferrer, J.: Appraisal of steamflood models. Rev. Tec Ing. **9**, 45–58 (1986)
2. Adegbesan, K.O., Donnelly, J.K., Moore, R.G., Bennion, D.W.: Low-temperature oxidation kinetic parameters for in-situ combustion numerical simulation. SPE Reserv. Eng. **2**, 573–582 (1987)
3. Akkutlu, I.Y., Yortsos, Y.C.: The dynamics of in-situ combustion fronts in porous media. Combustion and Flame **134**, 229–247 (2003)
4. Akkutlu, I.Y., Yortsos, Y.C.: Steady-state propagation of in-situ combustion fronts with sequential reactions. In: SPE International Petroleum Conference in Mexico. Society of Petroleum Engineers (2004)
5. Alexander, J., Martin, W.L., Dew, J.: Factors affecting fuel availability and composition during in situ combustion. J. Petrol. Tech. **14**(10), 1154–1164 (1962)
6. Belgrave, J.D.M., Moore, R.G.: A model for improved analysis of in-situ combustion tube tests. J. Pet. Sci. Eng. **8**(2), 75–88 (1992)
7. Bruining, J., Mailybaev, A.A., Marchesin, D.: Filtration combustion in wet porous medium. SIAM J. Appl Math. **70**, 1157–1177 (2009)
8. Castanier, L.M., Brigham, W.E.: Modifying in-situ combustion with metallic additives. In Situ **21**(1), 27–45 (1997)
9. Castanier, L.M., Brigham, W.E.: Upgrading of crude oil via in situ combustion. J. Pet. Sci. Eng. **39**, 125–136 (2003)
10. Chapiro, G., Mailybaev, A.A., de Souza, A.J., Marchesin, D., Bruining, J.: Asymptotic approximation of long-time solution for low-temperature filtration combustion. Comput. Geosci. **16**(3), 799–808 (2012)
11. Crookston, R., Culham, W., Chen, W.: A numerical simulation model for thermal recovery processes. Soc. Pet. Eng. J. **19**(01), 37–58 (1979)
12. Fassihi, M., Brigham, W., Ramey Jr., H.: Reaction kinetics of in-situ combustion Part 1-observations. Old SPE Journal **24**(4), 399–407 (1984)
13. Freitag, N.P., Verkoczy, B.: Low-temperature oxidation of oils in terms of SARA fractions: why simple reaction models don't work. J. Can. Pet. Technol. **44**(3), 54–61 (2005)

14. Germain, P., Geyelin, J.L.: Air injection into a light oil reservoir: the horse creek project. In: Middle East Oil Show and Conference, Bahrain (1997)
15. Gerritsen, M., Kovscek, A., Castanier, L., Nilsson, J., Younis, R., He, B.: Experimental investigation and high resolution simulator of in-situ combustion processes; 1. Simulator design and improved combustion with metallic additives. In: SPE International Thermal Operations and Heavy Oil Symposium and Western Regional Meeting (2004)
16. Greaves, M., Ren, S., Rathbone, R., Fishlock, T., Ireland, R.: Improved residual light oil recovery by air injection (LTO process). J. Can. Pet. Technol. **39**(1) (2000)
17. Greaves, M., Young, T.J., El-Usta, S., Rathbone, R.R., Ren, S.R., Xia, T.X.: Air injection into light and medium heavy oil reservoirs: combustion tube studies on west of Shetlands Clair oil and light Australian oil. Chem. Eng. Res. Des. **78**(5), 721–730 (2000)
18. Gutierrez, D., Skoreyko, F., Moore, R., Mehta, S., Ursenbach, M.: The challenge of predicting field performance of air injection projects based on laboratory and numerical modelling. J. Can. Pet. Technol. **48**(4), 23–33 (2009)
19. Hardy, W.C., Fletcher, P.B., Shepard, J.C., Dittman, E.W., Zadow, D.W.: In-situ combustion in a thin reservoir containing high-gravity oil. J. Pet. Technol. **24**(2), 199–208 (1972)
20. Khoshnevis, N., Mailybaev, A.A., Bruining, J., Marchesin, D.: Effects of water on light oil recovery by air injection. Fuel **137**, 200–210 (2014)
21. Khoshnevis, N., Mailybaev, A.A., Marchesin, D., Bruining, J.: Compositional effects in light oil recovery by air injection: vaporization vs. combustion. Journal of Porous Media **17**, 937–952 (2014)
22. Khoshnevis, N., Mailybaev, A.A., Marchesin, D., Bruining, J., Recovery of light oil by air injection at medium temperature Experiments: J. Pet. Sci. Eng. **133**, 29–39 (2015)
23. Khoshnevis Gargar, N., Mailybaev, A.A., Marchesin, D., Bruining, H.: Diffusive effects on recovery of light oil by medium temperature oxidation. Transp. Porous Media **105**(1), 191–209 (2014)
24. Kok, M.V., Karacan, C.O.: Behavior and effect of SARA fractions of oil during combustion. SPE Reserv. Eval. Eng. **3**, 380–385 (2000)
25. Levenspiel, O.: Chemical Reaction Engineering. Wiley (1999)
26. LeVeque, R.: Finite Difference Methods for Ordinary and Partial Differential Equations: Steady-State and Time-Dependent problems. SIAM, Philadelphia (2007)
27. Lin, C.Y., Chen, W.H., Culham, W.E.: New kinetic models for thermal cracking of crude oils in in-situ combustion processes. SPE Reserv. Eng. **2**, 54–66 (1987)
28. Lin, C.Y., Chen, W.H., Lee, S.T., Culham, W.E.: Numerical simulation of combustion tube experiments and the associated kinetics of in-situ combustion processes. SPE J. **24**, 657–666 (1984)
29. Liu, H., Ni, Q.: Incomplete Jacobian Newton method for nonlinear equations. Comput. Math. Appl. **56**(1), 218–227 (2008)
30. Mailybaev, A.A., Bruining, J., Marchesin, D.: Analysis of in situ combustion of oil with pyrolysis and vaporization. Combust. Flame **158**(6), 1097–1108 (2011)
31. Mailybaev, Bruining, J., Marchesin, D.: Analytical formulas for in-situ combustion. SPE J. **16**(03), 513–523 (2011)
32. Mailybaev, A.A., Bruining, J., Marchesin, D.: Recovery of light oil by medium temperature oxidation. Transp. Porous Media **97**, 317–343 (2013)
33. Mailybaev, A.A., Marchesin, D., Bruining, J.: Resonance in low-temperature oxidation waves for porous media. SIAM J. Math. Anal. **43**, 2230–2252 (2011)
34. Poling, B.E., Prausnitz, J.M., John Paul, O.C., Reid, R.C.: The Properties of Gases and Liquids. McGraw-Hill, New York (2001)
35. Prigogine, I.: Introduction to thermodynamics of irreversible processes. Wiley (1967)
36. Xu, Z., Jianyi, L., Liangtian, S., Shilun, L., Weihua, L.: Research on the mechanisms of enhancing recovery of light-oil reservoir by air-injected low-temperature oxidation technique. Nat. Gas Ind. **24**, 78–80 (2004)
37. Youngren, G.: Development and application of an in-situ combustion reservoir simulator. Soc. Pet. Eng. J. **20**(01), 39–51 (1980)